Environ. Sci. Technol. **1997**, *31*, 1890−1897

Aromatics, Reformulated Gasoline, and Atmospheric Organic Aerosol Formation

J. R. ODUM,[†] T. P. W. JUNGKAMP,[†] R. J. GRIFFIN,[‡] H. J. L. FORSTNER,[‡] R. C. FLAGAN,[‡] AND J. H. SEINFELD*,[‡]

Environmental Engineering Science and Chemical Engineering, California Institute of Technology, Pasadena, California 91125

Secondary organic aerosol (SOA) yield curves have been obtained for 17 individual aromatic species from an extensive series of sunlight-irradiated smog chamber experiments. These yield curves, interpreted within the framework of a gas/aerosol absorption model, are used to quantitatively account for the SOA that is formed in a series of smog chamber experiments performed with the whole vapor of 12 different reformulated gasolines. The total amount of secondary organic aerosol produced from the atmospheric oxidation of whole gasoline vapor can be represented as the sum of the contributions of the individual aromatic molecular constituents of the fuel.

Introduction

Urban fine particulate matter is comprised of a complex mixture of both primary and secondary organic and inorganic compounds and emanates from a wide variety of sources. An important source that can significantly contribute to the fine particulate burden, especially during severe urban smog episodes, is secondary organic aerosol (SOA) (*1*−*5*). Much like ozone, secondary organic aerosol results from the atmospheric oxidation of reactive organic gases (ROGs). Whereas the oxidation of most ROGs results in ozone formation, SOA is generally formed only from the oxidation of ROGs comprised of seven or more carbon atoms, because oxidation products must have vapor pressures that are sufficiently low to enable them to partition into the aerosol phase (*1*, *2*).

The chemical reaction pathways of large ROG molecules are complex, and resulting oxidation products are both numerous and difficult to quantify analytically. As a result, it is currently not possible, ab initio, to determine the aerosol formation potential of individual ROGs and their contribution to the secondary organic urban particulate burden. However, a number of indirect methods have been employed to estimate the fraction of urban particulate carbon that is of secondary origin. Turpin and Huntzicker (*3*), using measured ratios of elemental carbon to organic carbon, estimated that as much as 70% of the organic carbon in Claremont, CA, during a 1987 smog episode was secondary. Friedlander and co-workers (*4*, *5*), using chemical element mass balance methods, suggested that SOA represented more than 75% of the total organic aerosol in Pasadena, CA, in 1973. More recent estimates using chemical mass balance methods suggest that, on a yearly average, 20−30% of the fine organic particulate matter in the South Coast Air Basin may be SOA (*6*).

* To whom correspondence should be addressed; phone: 818-395-4635; fax: 818-585-1729; e-mail: john@aeolus.che.caltech.edu.
[†] Environmental Engineering Science.
[‡] Chemical Engineering.

Another approach that has been used to estimate the importance of SOA involves the use of experimentally measured secondary organic aerosol yields (Y). An SOA yield is a measure of the amount of aerosol that is produced from the atmospheric oxidation of an ROG and is defined as

$$Y = \frac{\Delta M_o}{\Delta \mathrm{ROG}} \tag{1}$$

where ΔM_o is the amount of aerosol produced (μg m^{-3}) for a given reacted amount of an ROG, ΔROG (μg m^{-3}). Traditionally yields have been measured in smog chamber studies where an individual ROG is placed in the chamber with an appropriate amount of nitrogen oxides and is photooxidized until the reaction is complete. The amount of aerosol produced for the amount of reacted ROG is used to calculate the aerosol yield.

Yields have been measured for dozens of individual ROGs by a host of researchers over the last 20 years (*7*−*14*). While it was believed that each ROG must possess a constant yield value, measured yields for an individual ROG have exhibited a wide degree of variation both between and within laboratories. Odum *et al.* offered a possible explanation for this variation by proposing a new framework within which to interpret SOA yield data (*15*). Rather than considering the aerosol formation process as a product supersaturation/condensation phenomena, Odum *et al.* suggested that secondary organic aerosol formation is best described by a gas/aerosol absorptive partitioning model (*15*−*17*). Within that framework, oxidation products, produced from the atmospheric oxidation of an ROG, are considered to be semivolatile and can partition themselves into an absorbing organic aerosol (om) phase at concentrations below their saturation concentrations. The partitioning of each semivolatile oxidation product is described by a partitioning coefficient ($K_{\mathrm{om},i}$) as

$$K_{\mathrm{om},i} = \frac{A_{\mathrm{om},i}}{G_i M_o} = \frac{760RT}{10^6 \mathrm{MW}_{\mathrm{om}} \zeta_i \, p^{\circ}_{\mathrm{L},i}} \tag{2}$$

where $A_{\mathrm{om},i}$ is the concentration of product i in the absorbing aerosol om phase (ng m^{-3}), G_i is the gas phase concentration of product i (ng m^{-3}), M_o is the absorbing organic aerosol mass concentration (μg m^{-3}), R is the ideal gas constant (8.206 $\times$ 10^{-5} m^3 atm mol^{-1} K^{-1}), T is the temperature (K), $\mathrm{MW}_{\mathrm{om}}$ is the mean molecular weight of the om phase, ζ_i is the activity coefficient of product i in the om phase, and $p^{\circ}_{\mathrm{L},i}$ is the vapor pressure of product i as a pure liquid (subcooled, if necessary).

Using the gas/aerosol absorption model to interpret yield data, Odum *et al.* showed that SOA yields for an individual ROG are not uniquely valued, but rather are a function of the available absorbing organic aerosol concentration (*15*):

$$Y = M_o \sum_i \left(\frac{\alpha_i K_{\mathrm{om},i}}{1 + K_{\mathrm{om},i} M_o} \right) \tag{3}$$

where α_i is the mass-based stoichiometric coefficient for the reaction generating product i (i.e., $1000\alpha_i\Delta\mathrm{ROG} = C_i$, where $C_i = A_{\mathrm{om},i} + G_i$). Assuming that there are two hypothetical products for each ROG, Odum *et al.* were successfully able to fit over 30 experimentally determined aerosol yields for three different ROGs (*m*-xylene, 1,2,4-trimethylbenzene, and α-pinene) (*15*). Hoffmann *et al.* were also able to use this partitioning theory to describe aerosol yields for eight different biogenic ROGs (*18*).

S0013-936X(96)00535-4 CCC: $14.00
© 1997 American Chemical Society

Nearly all of the smog chamber studies of secondary aerosol formation in the past have been conducted using only one ROG per experiment. However with the advent of an appropriate theory for SOA formation, the opportunity exists to study the aerosol formation potentials of complex ROG mixtures, in an attempt to more accurately mimic atmospheric SOA formation. In this paper, we discuss a series of 35 smog chamber experiments that were conducted on 17 individual alkylated aromatic species in order to determine the appropriate yield curves for these compounds. We also present data from a series of 20 smog chamber experiments that were conducted using the whole vapor of 12 different reformulated gasoline blends to determine those fuel parameters that control the aerosol formation potential of whole gasoline vapor. We then show that gas/aerosol absorption partitioning theory can be successfully applied to the SOA formation resulting from the atmospheric photooxidation of a complex mixture like whole gasoline vapor.

Experimental Description

Experiments were performed in a 60 m^3 sealed, collapsible Teflon bag that has been described in detail previously (*7, 8, 15*). Most of these experiments were conducted in a dual-chamber mode, in which the bag was divided in the center, so that two different experiments could be conducted under identical environmental (i.e., sunlight intensity, temperature, etc.) conditions. Prior to each experiment, the chamber was continuously flushed with purified laboratory compressed air for at least 38 h (4−5 bag volumes) and baked in sunlight for at least 1 day, as described in Odum *et al.* (*15*).

Hydrocarbon measurements were made using a Hewlett Packard (Palo Alto, CA) 5890 gas chromatograph (GC) that was equipped with an HP-1 capillary column (20 m × 0.1 mm × 0.1 μm film thickness, Hewlett Packard) and a flame ionization detector (FID). The GC temperature program was as follows: −60 °C for 1 min, −60 to 50 °C at 40 °C min^{-1}, 50 to 70 °C at 5 °C min^{-1}, and 70 to 225 °C at 40 °C min^{-1}. Hydrocarbon calibrations were performed prior to each experiment by vaporizing microliter volumes of a calibration solution into a 60-L Teflon bag filled with a measured volume of Ultra Zero (Air Liquid America Corp., Houston, TX) compressed air. For each of the gasoline runs, a calibration solution containing methyl *tert*-butyl ether, 2-methylpentane, 3-methylpentane, 2,2,4-trimethylpentane, toluene, ethylbenzene, *o*-xylene, and 1,2,4-trimethylbenzene was used.

The calibrations were followed by injection of $(NH_4)_2SO_4$ seed particles into the smog chamber to attain particle concentrations of 5000−10 000 particles cm^{-3} with a number mean diameter of approximately 100 nm. The particles were generated by atomizing an aqueous solution of $(NH_4)_2SO_4$ using a stainless steel, constant rate atomizer. The aerosol was passed through heated copper tubing into a diffusional dryer, followed by a ^{85}Kr charge neutralizer before entering the chamber.

After obtaining the desired initial seed particle concentration, propene, hydrocarbons, NO_x, and hexafluorobenzene (C_6F_6) were injected (approximately 1 h prior to the start of the experiment) through Teflon lines into the chamber, which was completely shrouded from sunlight with a black polyethylene tarpaulin. Propene, NO, and NO_2 were injected using certified cylinders containing approximately 500 ppm of the gas in nitrogen. Hydrocarbons and C_6F_6 were introduced into the chamber by injecting microliter quantities of the pure liquid into a glass bulb that was gently heated while being diluted with purified compressed lab air that went directly to the chamber. Propene was used at mixing ratios of 250−350 ppb to facilitate the production of hydroxyl (OH) radicals in sufficient concentrations for the inception of the experiment. The C_6F_6 was used as an internal standard for hydrocarbon gas chromatographic (GC) samples in order to normalize for injection variations of the six-port stainless steel injection valve (Valco, Houston, TX), equipped with a heated (100 °C) 2-mL Teflon sampling loop. The use of the internal standard yielded estimated uncertainties in the hydrocarbon measurements of less than ±2% for most experiments.

After injection of the gases and seed aerosol, but before uncovering the chamber, initial measurements of hydrocarbons, NO_x, O_3, and aerosol concentrations and size distributions were made to obtain initial values and to ensure that the contents were well mixed. Generally three to five initial hydrocarbon measurements, using the HP 5890 GC described above, were made for each side of the bag. A Thermo Environmental Instruments (Franklin, MA) Model 42 chemiluminescence NO_x monitor was used to measure NO, NO_2, and NO_x. Complete NO_x monitor calibrations were performed daily. A Dasibi Environmental Corp. (Glendale, CA) Model 1008-PC O_3 analyzer was used to monitor O_3 concentrations. NO_x and O_3 measurements were made at 10-min intervals between alternating sides of the chamber. Estimated uncertainties in the NO and NO_2 measurements are approximately ±4% and ±7%, respectively. The ozone instrument has an estimated uncertainty of ±4% in its initial calibration and was seen to drift only a few percent over the period of several months.

Complete number and size distribution measurements were recorded for both sides of the chamber with a 1-min frequency throughout an experiment. The aerosol instrumentation consisted of one TSI Model 3071 cylindrical scanning electrical mobility spectrometer for each side of the divided chamber. Each electrical mobility spectrometer (SEMS) was equipped with a TSI Model 3760 condensation nuclei counter (CNC) to count transmitted particles. SEMS voltages were scanned from 40 to 8500 V with a 1-min ramp. The cylindrical SEMS were operated with sheath and excess flows of 2.5 L min^{-1} and inlet and classified aerosol flows of 0.25 L min^{-1} to allow for measurement of particle size distributions in the range of 30−850 nm. A more complete description of the SEMS scanning cycle and operation have been published previously (*8*). Particle losses in the SEMS, SEMS response functions, particle charging efficiencies, CNC counting efficiency, and particle deposition in the chamber have been taken into account in the analysis of the aerosol data (*8*). Estimated uncertainties in the SEMS size and concentration measurements are approximately ±10%.

After making initial measurements prior to the start of the experiment, the black tarpaulin (chamber cover) was removed to expose the chamber contents to sunlight. Hydrocarbon measurements were made for both sides of the chamber every 8−10 min throughout the experiment. NO, NO_2, NO_x, and O_3, were continuously monitored during 10-min intervals alternating between the two sides of the chamber. Temperature, total solar radiation, and UV were continuously monitored over the course of the experiment.

All gasoline blends used in this study were produced during the Auto/Oil Air Quality Improvement Program (AQIRP). The Auto/Oil industry AQIRP was a study conducted by 14 petroleum companies and the three domestic automakers; their prime objective was to examine the potential improvements in vehicle emissions and, ultimately, air quality from reformulated gasoline (*19, 20*). The AQIRP produced over 80 different fuel blends in which specific fuel properties were controlled. Detailed chemical speciation/quantitation was performed on all of the AQIRP fuels during that program (*21, 22*). For the individual aromatic smog chamber experiments, the concentration−time profile of the hydrocarbon was explicitly determined from GC/FID peak areas and calibration data. For the gasoline experiments, only the eight calibration species mentioned above were explicitly tracked using the GC/FID. Initial concentrations of the eight calibration species for the gasolines were measured for each experiment. Knowing the mass percent of every compound in a fuel

TABLE 1. Conditions for Individual Aromatic Experiments

date	compound	$[ROG]_o$ ($\mu g\ m^{-3}$)	$[NO]_o$ (ppb)	$[NO_2]_o$ (ppb)	T_{avg} (K)	ΔROG ($\mu g\ m^{-3}$)	ΔM_o ($\mu g\ m^{-3}$)	Y
06/06/96a	*m*-ethyltoluene	2141	510	240	307	1927	208	0.108
06/06/96b	*m*-xylene	2017	415	185	307	1891	106	0.056
06/12/96a	1,3,5-trimethylbenzene	1029	280	105	304	1029	31	0.031
06/12/96b	*m*-ethyltoluene	1091	265	97	304	971	66	0.068
06/17/96a	ethylbenzene	4011	989	460	306	434	13	0.030
06/17/96b	*m*-ethyltoluene	415	96	47	306	334	13	0.039
06/19/96a	*m*-xylene	1596	306	136	304	1571	46	0.029
06/19/96b	*m*-xylene	1596	287	127	304	1528	48	0.031
06/21/96a	ethylbenzene	6733	484	260	301	3176	394	0.124
06/21/96b	*p*-diethylbenzene	488	115	93	301	314	17	0.055
06/24/96a	ethylbenzene	3696	255	167	302	1872	185	0.099
06/24/96b	*p*-diethylbenzene	1137	166	106	302	742	61	0.082
06/28/96a	toluene	2560	443	242	303	1413	133	0.094
06/28/96b	*p*-xylene	1163	228	142	303	823	16	0.019
07/01/96a	toluene	2415	200	145	315	1268	111	0.088
07/01/96b	*p*-xylene	1399	210	171	315	1063	32	0.030
07/05/96a	toluene	2656	488	305	312	1710	171	0.100
07/05/96b	*n*-propylbenzene	4314	507	316	312	1314	103	0.078
07/08/96a	*p*-ethyltoluene	998	166	110	308	708	38	0.054
07/08/96b	*o*-ethyltoluene	1131	166	113	308	789	49	0.062
07/10/96a	ethylbenzene	3514	185	119	307	1169	104	0.089
07/10/96b	toluene	3065	149	104	307	923	68	0.074
07/12/96a	1-methyl-3-*n*-propylbenzene	1389	409	200	309	1220	72	0.059
07/12/96b	1,2-dimethyl-4-ethylbenzene	1463	376	210	309	1426	49	0.034
07/15/96a	1,2-dimethyl-4-ethylbenzene	1681	440	232	309	1602	72	0.045
07/15/96b	1-methyl-3-*n*-propylbenzene	1179	254	149	309	1041	54	0.052
07/17/96a	*n*-propylbenzene	1862	260	158	307	657	39	0.059
07/17/96b	1,2,4,5-tetramethylbenzene	1426	406	230	307	1394	40	0.029
07/19/96a	*n*-propylbenzene	5398	409	259	312	1790	190	0.106
07/19/96b	1,2,4,5-tetramethylbenzene	2339	635	354	312	2339	70	0.030
07/22/96	1,4-dimethyl-2-ethylbenzene	1245	335	185	313	1251	50	0.040
09/09/96	*o*-xylene	1403	368	188	312	1117	35	0.031
09/11/96	*o*-xylene	1779	511	266	310	1082	23	0.021
09/16/96a	1,2,3,5-tetramethylbenzene	2427	701	345	302	2142	65	0.030
09/16/96b	1,2,3,5-tetramethylbenzene	1270	368	185	302	1071	25	0.023

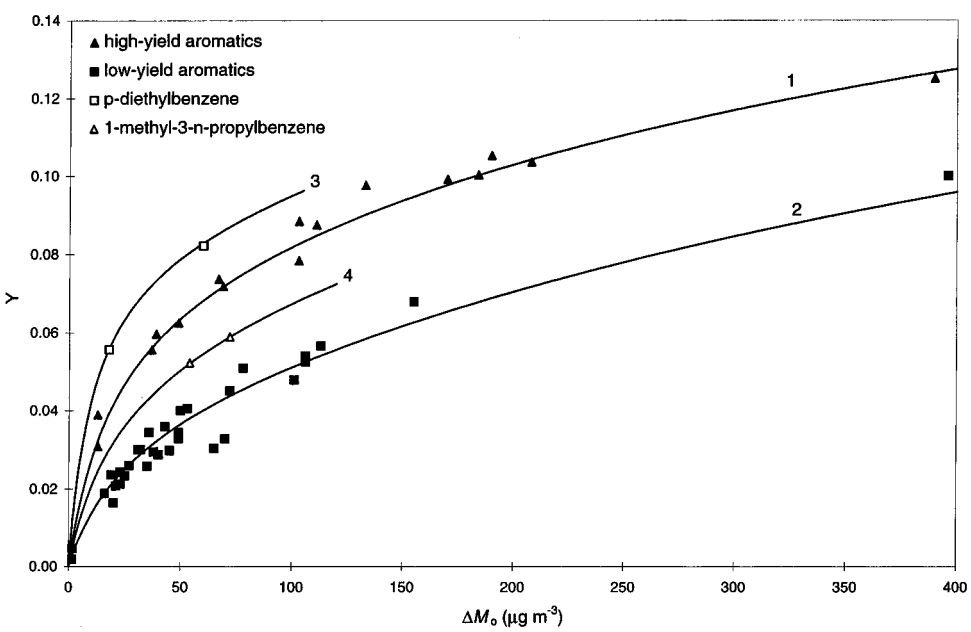

FIGURE 1. Secondary organic aerosol yields as a function of organic aerosol mass concentration (ΔM_o) for 17 individual aromatic species. Each data point represents an individual experiment. Curves are fit to the data using a two-product model in conjunction with eq 3 by minimizing the weighted squared residuals. Curve 1 is fit with the values 0.038, 0.042, 0.167, and 0.0014 for α_1, $K_{om,1}$, α_2, and $K_{om,2}$, respectively. The corresponding values are 0.071, 0.053, 0.138, and 0.0019 for curve 2; 0.083, 0.093, 0.22, and 0.0010 for curve 3; and 0.05, 0.054, 0.136, and 0.002 for curve 4.

(obtained from AQIRP speciation data) allowed the initial concentration of all species to be calculated from the initial concentrations of the eight calibration species. Then by measuring the concentration−time profiles of the eight calibration species and knowing their reaction rate constants with hydroxyl radical, a concentration−time profile for OH was calculated for each experiment. Typical calculated OH concentrations ranged from 1×10^6 to 5×10^6 molecule cm^{-3}. This, along with the measured ozone (O_3) concentrations and OH and O_3 rate constants, was used to calculate the

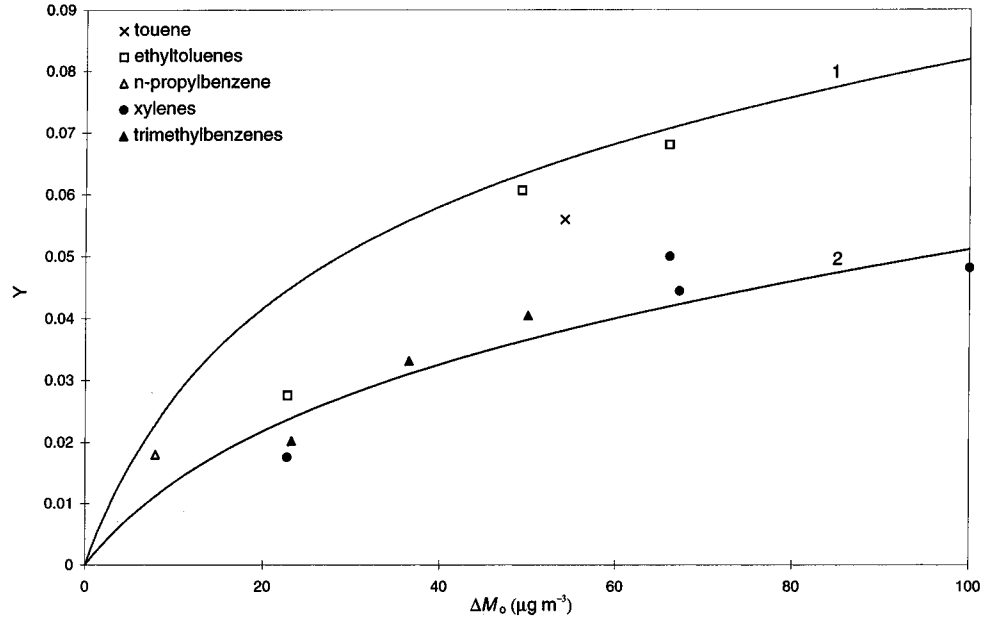

FIGURE 2. Secondary organic aerosol yield data of Izumi and Fukuyama (*10*) analyzed within the absorption model framework. Curves 1 and 2 from Figure 1 are shown for comparison.

TABLE 2. Properties of AQIRP Reformulated Gasolines[a]

fuel code/AQIRP phase	fuel ID	aromatics (vol %)	MTBE (vol %)	olefins (vol %)	T_{90} (°F)
A/l	industry average	32.0	0.0	9.2	330
F/l	amot	20.0	0.0	3.2	279
G/l	AmOt	44.3	0.0	17.4	286
K/l	Amot	45.7	0.0	4.9	294
L/l	AmOT	47.8	0.0	17.7	357
O/l	AMOt	46.7	14.6	19.3	283
P/l	amOt	20.3	0.0	18.3	284
C2/II	Cal Phs II	25.4	11.2	4.1	293
1B/II	matrix B Base	25.3	11.2	15.0	267
2B/II	base + RMH	35.1	10.4	11.2	314
3B/II	base + AH	22.1	10.4	13.3	299
4B/II	base + AH + RMH	32.2	10.2	10.7	334

[a] A/a, high/low aromatics; M/m, high/low MTBE; O/o, high/low olefins; T/t, high/low T_{90} (90% distillation temperature); RMH, medium and heavy reformate cut (predominantly C_9 and C_{10} aromatics); AH, heavy alkylate cut (heavy paraffins).

concentration−time profile for each speciated compound in a fuel.

Hydroxyl radical and ozone reaction rate constants for the speciated compounds were obtained either from the literature (*23*) and NIST chemical kinetic database (*24*) or when experimentally not known were estimated using structure−reactivity relationships (*25*). Whereas the structure−reactivity relationship (SAR) expressions for alkanes and alkenes were used unchanged, those for the aromatic species were modified. The Hammet substituent constant σ_m^+ used in the SAR expression had to be optimized for alkyl-substituted aromatics, since the values in the range of $\sigma_m^+ \sim -0.06$ derived originally for different alkyl substituents by Brown and Okamoto (*26*) lead to spurious results for those aromatics with a substitution pattern of alkyl groups in the *meta*-position. Experimentally known OH overall reaction rate constants (*23*) for 15 alkyl-substituted aromatics were used to derive ring addition rate constants k^{add}. The contribution of side chain reactivity to the experimental values was accounted for by subtracting the SAR estimates of OH abstraction rate constants. Predicted addition rate constants obtained by the Hammet expression were fit to the experimental k^{add} rates by minimizing the sum of square error varying the value of σ_m^+, taken to be uniform for the various alkyl substituents. The optimized expression for OH addition rate constant $\log_{10} k^{add}$ (cm^3 molecule^{-1} s^{-1}) $= -11.89 - 1.82\sum\sigma^+$ was obtained with $\sigma_m^+ = -0.190$ for alkyl substituents and $\sigma_{o,p}^+$ as used in ref 25. The quality of the fit for the overall OH radical rate constant estimates for the aromatics was improved to 30% maximum error as compared to 110% using the parameters in ref 25.

Aromatic Aerosol Yields

A series of 35 smog chamber experiments were performed with 17 individual aromatic species to determine the SOA yields for these individual compounds. Table 1 lists the experimental conditions and results for each smog chamber run. The total organic aerosol mass concentration produced (ΔM_o) and the total concentration of aromatic consumed (ΔROG) in each experiment were measured and used to calculate the SOA yield ($Y = \Delta M_o/\Delta$ROG) for each experiment. These individual aromatic aerosol yields are shown as a function of ΔM_o in Figure 1. In general, the data falls into two distinct classes, which we have labeled low-yield and high-yield aromatics. The high-yield aromatic species are those species containing one or fewer methyl substituent and one or fewer ethyl substituent (i.e., toluene, ethylbenzene, and ethyltoluenes) as well as *n*-propylbenzene. The low-yield aromatics are those aromatics that contain two or more methyl substituents (i.e., xylenes, trimethylbenzenes, dimethylethylbenzenes, tetramethylbenzenes). Eighteen of the low-yield aromatic points are from experiments conducted

TABLE 3. Conditions for Gasoline Experiments

experiment	fuel	$[ROG]_o$ ($\mu g\ m^{-3}$)	$[NO]_o$ (ppb)	$NO_{2]o}$ (ppb)	chamber T_{avg} (K)
07/26/96a	C2	7179	950	476	315
07/26/96b	RF-A	6603	926	480	315
07/29/96a	RF-A	6926	1038	529	315
07/29/96b	C2	8595	953	490	315
08/19/96a	RF-L	3421	845	424	310
08/21/96a	RF-A	3756	469	256	313
08/21/96b	RF-F	5457	930	460	313
08/23/96b	RF-L	2733	456	250	313
08/26/96a	RF-F	6217	1011	498	311
08/26/96b	RF-G	6042	987	511	311
08/28/96a	RF-1B	5855	957	517	315
08/28/96b	RF-3B	5371	955	516	315
08/30/96a	RF-2B	6377	1046	570	314
08/30/96b	RF-4B	5019	903	456	314
09/02/96a	RF-G	5991	940	495	309
09/02/96b	RF-O	6326	989	533	309
09/04/96a	RF-P	6759	1068	550	308
09/04/96b	RF-F	5999	878	453	308
09/06/96a	RF-K	6528	1007	500	310
09/06/96b	C2	6561	916	468	310

in the Caltech smog chamber in the summer of 1995, the experimental conditions of which have been previously published (*15*). The curves through the data in Figure 1 have been generated using eq 3, assuming a hypothetical two-product model. That is, a set of α_1, α_2, $K_{om,1}$, and $K_{om,2}$ are chosen for each curve, and these values are adjusted to minimize the square of the residuals. Whereas the organic aerosol phase produced from the atmospheric oxidation of an individual aromatic is comprised of dozens of oxidation products (27), the yield data can be fit assuming that there are only two hypothetical products (i.e., four parameters). The use of only one model product (i.e., two parameters) is insufficient to capture the behavior of the data over the complete range of organic aerosol mass concentrations. While using three or more model products (i.e., six or more parameters) is superfluous.

Since the parent aromatics species corresponding to each of the curves in Figure 1 are similar in structure, it is highly likely that they generate similar atmospheric oxidation products. Indeed, Forstner et al. found that many individual aromatic species generate similar (and in some cases identical) atmospheric oxidation products (*27*). Therefore it does not seem surprising that much of the data in Figure 1 fall on only two yield curves. At present, we are not able to determine why compounds corresponding to curve 1 have higher yields than those corresponding to curve 2. One might speculate that the single-substituted aromatics (i.e., those on curve 1) might generate a higher ratio of ring-retaining to ring-cleavage products than the multiply-substituted aromatics (i.e., those on curve 2). Ring-retaining products may have lower vapor pressures than the smaller ring-cleavage products, resulting in higher yields for the single-substituted aromatics. However, in the absence of complete product information, it is difficult to definitively determine the correct explanation for this observation.

Another fairly comprehensive aromatic aerosol yield data set is that of Izumi and Fukuyama (*10*). Figure 2 shows this data set analyzed within the framework of the absorptive partitioning model outlined above. The yield curves shown in the figure are curves 1 and 2 from Figure 1. Although the fit is not perfect, the agreement between the data set of Izumi and Fukuyama and the curves generated from the Caltech data is quite striking. Thus it would seem that much of the variability seen in aerosol yield data sets in the literature can be accounted for if yields are interpreted within the gas/aerosol absorption model.

To predict the amount of SOA that is formed from the atmospheric oxidation of an ROG based on first principles would require complete knowledge of all the oxidation products, their stoichiometric reaction coefficients, their vapor pressures, and their activity coefficients in the om phase (i.e., see eqs 2 and 3). Whereas from a fundamental standpoint this would be the most satisfying approach, it is rather impractical given the current state of knowledge. Complete product information is not available for any aromatic parent species, and even if it were, estimating all the associated parameters would prove to be a formidable task. However, therein lies the power of yield curves like those shown in Figure 1. Using these curves, one can predict the amount of aerosol formed from the atmospheric oxidation of a mixture of these compounds, despite the lack of knowledge concerning oxidation products.

TABLE 4. Results for Gasoline Experiments

date	fuel	ΔROG ($\mu g\ m^{-3}$)	ΔAromatic ($\mu g\ m^{-3}$)	max O_3 (ppb)	actual ΔM_o ($\mu g\ m^{-3}$)	predicted ΔM_o ($\mu g\ m^{-3}$)	pred/actual
7/26/96	RF-A	3642	1742	1668	160	113	0.71
7/29/96	RF-A	3554	1725	1733	110	94	0.85
8/21/96	RF-A	2601	1178	1248	64	53	0.83
7/26/96	C2	3203	1200	1536	36	47	1.31
7/29/96	C2	3551	1421	1687	54	63	1.17
9/06/96	C2	2072	814	1012	18	21	1.17
8/19/96	RF-L	1876	907	1156	130	60	0.46
8/23/96	RF-L	1784	846	1269	95	52	0.55
8/21/96	RF-F	2326	823	1084	22	26	1.18
8/26/96	RF-F	1826	627	540	18	17	0.97
9/04/96	RF-F	1648	551	469	15	13	0.87
8/26/96	RF-G	3088	1407	1476	110	98	0.89
9/02/96	RF-G	3134	1459	1484	108	102	0.94
9/06/96	RF-K	2638	1409	1328	84	90	1.07
9/02/96	RF-O	3348	1549	1479	118	115	0.97
9/04/96	RF-P	2918	777	1371	35	29	0.83
8/28/96	RF-1B	2663	788	1513	28	28	1.00
8/30/96	RF-2B	3273	1556	1595	64	76	1.19
8/28/96	RF-3B	2243	678	1482	17	18	1.06
8/30/96	RF-4B	2534	1270	1564	56	58	1.04
						av =	1.00 ± 0.16

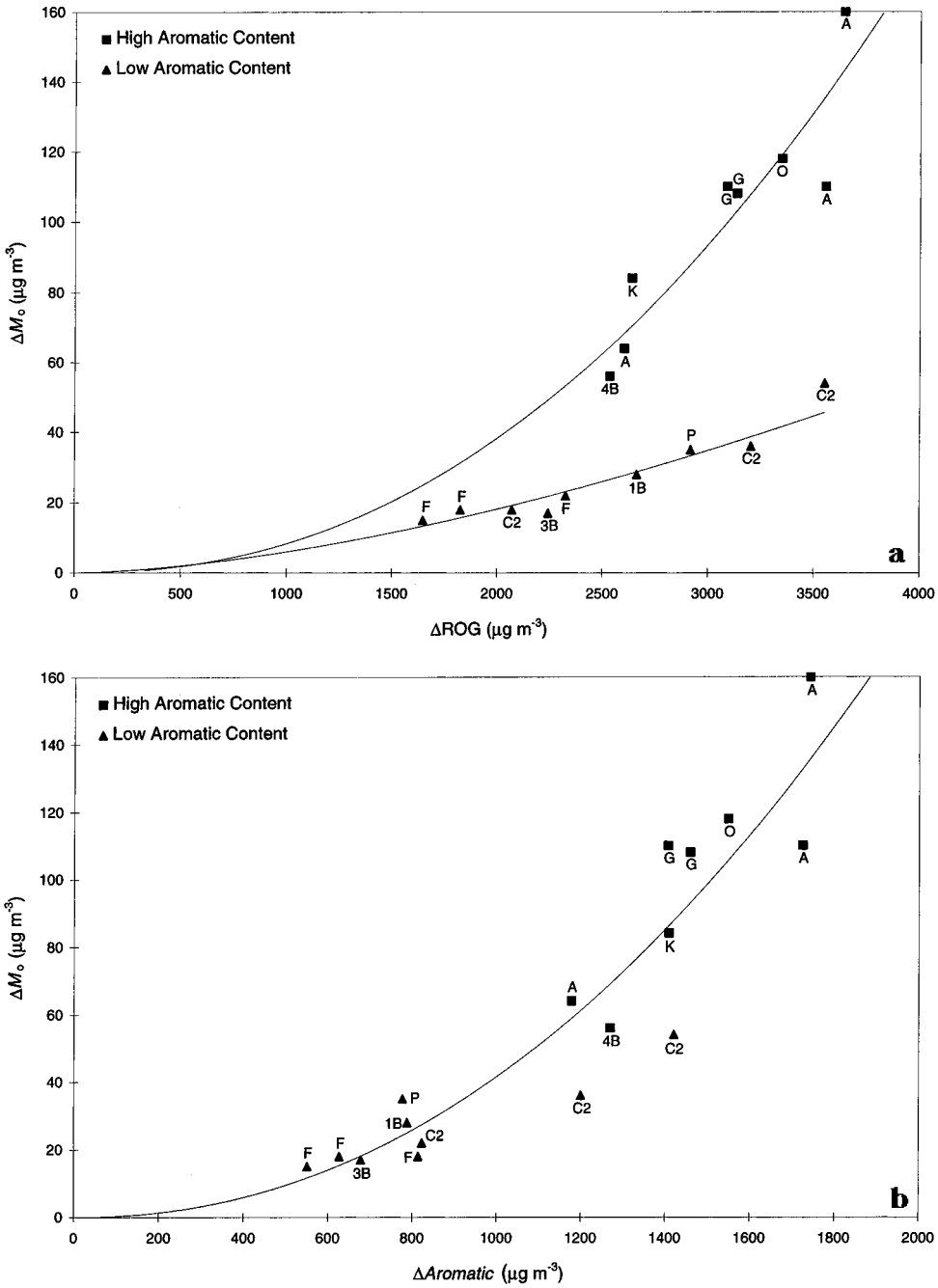

FIGURE 3. (a) Concentration of secondary organic aerosol mass formed (ΔM_o) as a function of the total reacted gas concentration (ΔROG) for AQIRP fuels. Power law fits to the data are solely for purposes of aiding the eye. (b) Concentration of secondary organic aerosol mass formed (ΔM_o) as a function of the total reacted aromatic concentration (ΔAromatic) for AQIRP fuels. Power law fit to the data is solely for purposes of aiding the eye.

Aerosol Formation Potentials of Whole Gasoline Vapor

A series of 20 smog chamber experiments using 12 different reformulated gasolines obtained from the Auto/Oil Air Quality Improvement Research Program (AQIRP) were performed to determine those fuel properties (e.g., % aromatics, % olefins, T_{90} distillation temperature, etc.) that are important for predicting the atmospheric aerosol formation potential of the whole fuel vapor. The 12 fuels used in this study and some of their controlled properties are listed in Table 2.

Experimental conditions and results for the gasoline smog chamber runs are listed in Tables 3 and 4. In Figure 3a, the organic aerosol concentration (ΔM_o) produced from the atmospheric oxidation of whole gasoline vapor is shown as a function of the total reacted organic gas concentration (ΔROG). The most striking feature of this figure is that the data points fall into two distinct classes. The high aromatic content fuels (32% ≤ % aromatic < 48%) produce significantly more aerosol for the same amount of total reacted organic gas than the low aromatic content fuels (20% ≤ % aromatic < 25.5%). This suggests that aromatic content is an important parameter influencing the amount of organic aerosol that is produced from the atmospheric oxidation of whole gasoline vapor. Indeed, if ΔM_o is instead plotted against the total amount of aromatics that reacted during the oxidation of a fuel (ΔAromatic), as is shown in Figure 3b, the data collapse onto a single curve.

A second interesting feature to note in Figure 3 is that the curves through the data are nonlinear. This results from the fact that SOA yields increase as a function of ΔM_o as shown by eq 3 and Figure 1. In other words, as more hydrocarbon

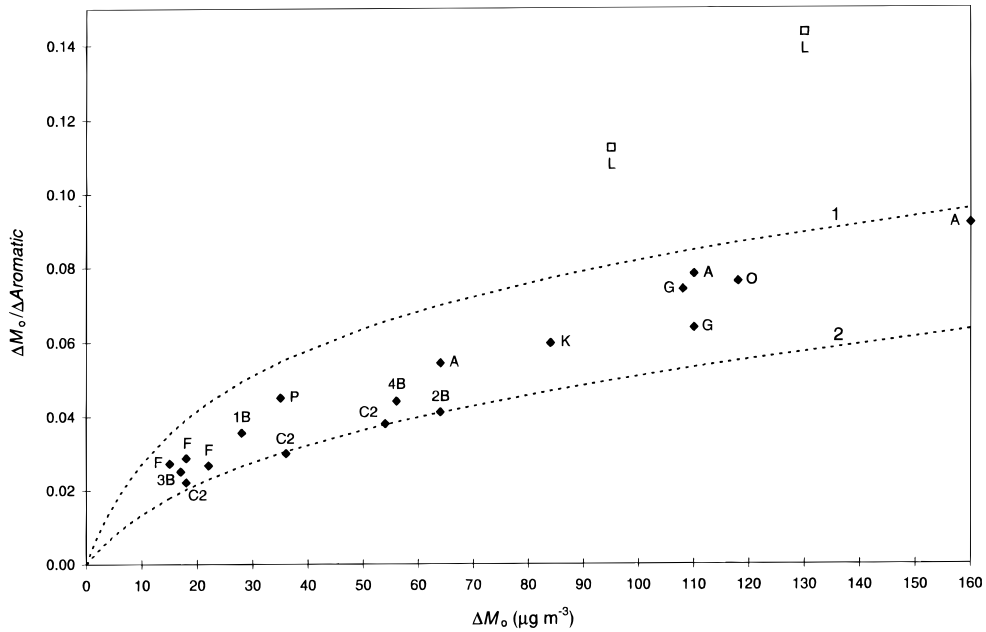

FIGURE 4. $\Delta M_o/\Delta$Aromatic as a function of ΔM_o for AQIRP fuels. Curves 1 and 2 are taken from Figure 1. Reprinted by permission of the American Association for the Advancement of Science (*29*).

reacts, producing more organic aerosol, a larger mass fraction of each semivolatile oxidation product will partition to the aerosol phase. This effect is clearly demonstrated in Figure 4 where $\Delta M_o/\Delta$Aromatic is shown as a function of ΔM_o. Curves 1 and 2 from Figure 1 have been included as well. The ratio $\Delta M_o/\Delta$Aromatic is a measure of the SOA yield from the aromatic fraction of the fuel. Indeed, for the individual aromatic curves $\Delta M_o/\Delta\text{Aromatic} = Y$. As eq 3 predicts, the value of the "yield" increases as a function of ΔM_o. More importantly however, data points for all fuels, other than fuel RF-L, fall within the range defined by curves 1 and 2. This strongly re-enforces the point that aromatics are the class of compounds that are responsible for producing the majority of the SOA formed during the atmospheric oxidation of whole gasoline vapor. If significant amounts of SOA were being produced by other classes of compounds (i.e., olefins, alkanes, and oxygenates) present in the fuels, then most points would lie above the envelope defined by curves 1 and 2.

For most of the fuels, between 92 and 99% of the mass of each fuel was speciated in AQIRP. However only 83% of the mass of fuel RF-L, which was the only high T_{90} fuel from phase I of AQIRP used in this study, was speciated in AQIRP. The 90% distallation temperature, T_{90}, of a fuel relates to the fuel's heavy-end volatilty. Fuels with large T_{90} values contain a larger fraction of heavier species. Many of these heavier species are C_{10}−C_{12} aromatics that were not speciated in phase I of AQIRP. Thus, much of the remaining 17% of the mass that was not speciated for fuel RF-L is most likely heavy aromatic species that contribute to the SOA formed from the oxidation of this fuel. Since this 17% was not speciated, its contribution to ΔAromatic could not be estimated. Thus ΔAromatic is most likely underestimated and is the reason that this fuel does not fall within the envelope as all other fuels in Figure 4.

Determining that aromatics clearly control the aerosol formation potential of whole gasoline vapor presents the opportunity to quantitatively predict the SOA formed during its atmospheric oxidation. Even though yield curves are not available for every aromatic species present in the fuels, using the curves for the 17 species in Figure 1, along with the observation that all isomers of a given compound seem to be described by the same yield curve, yield curves are available for 19 of the 26 aromatics that were speciated in phase I of AQIRP. These 19 species represented, on average, 96% of ΔAromatic for all fuels other than RF-A and RF-L. Of the 57 aromatic compounds that were speciated for the AQIRP phase II fuels, yield curves are available for 28 species representing, on average, 95% of ΔAromatic. Obtaining yield values for each aromatic from the curves in Figure 1, corresponding to the amount of SOA formed (ΔM_o) in an individual experiment and multiplying these values by the reacted amount of the respective aromatic, yields an estimate of the amount of SOA that is attributable to each of the aromatic species. Summing these values for all aromatics in a given fuel for a given experiment gives a quantitative estimate of the amount of SOA that was produced by the aromatic fraction of each fuel in a given experiment. Table 4 lists the observed total SOA concentration produced from the atmospheric oxidation of the whole gasoline vapor as well as the total SOA predicted to be formed solely from the aromatic fraction of the fuel. This method accounts for 70−130% of the SOA that was produced for all fuels other than fuel RF-L. The average for all fuels, excluding RF-L, is 100 ± 16% (1σ). Thus, by simply accounting for the aerosol formation potential of a fuel's aromatic content, one can quantitatively account for the SOA formed from the atmospheric oxidation of whole gasoline vapor.

Besides RF-L, of the 12 fuels listed in Table 4, industry average (RF-A) is accounted for with the lowest level of accuracy. The SOA predicted to be formed from industry average is consistently underpredicted. This most likely results from the fact that RF-A contains a significant fraction of heavy aromatics for which no yield curves are available. These aromatics include naphthalene, methylnaphthalenes, indan, and methylindans. These compounds most certainly have substantial aerosol forming potentials and thus would significantly contribute to the SOA formed from this fuel. However at present, aerosol yield curves are not available for these compounds, and thus their contribution to the SOA formed could not be included in the calculations. Despite this problem, however, this amounts to an average underprediction of only 20% ($n = 3$) for this fuel, which is certainly adequate for atmospheric modeling purposes. Considering that whole gasoline vapor is comprised of over 300 chemical species, it is striking that the aerosol formed from its atmospheric oxidation can be accounted for using the methods described above with such accuracy. These results

certainly suggest that it is highly likely that SOA formation in an urban airshed can be modeled using yield data like that presented in this paper.

California phase II and Industry Average. Two experiments were performed in which California phase II (C2) and industry average (RF-A) gasoline were placed in opposing sides of the chamber so that the aerosol forming potential of the two fuels could be examined simultaneously under identical environmental conditions. The most interesting of this series is the experiment performed on 7/29/96. The initial concentration of RF-A on side A of the chamber was 6926 μg m^{-3}, and C2 on side B of the chamber was 8595 μg m^{-3}. Despite the much larger initial concentration of C2, the total amount of ROG that reacted (ΔROG) was identical for the two fuels (see Table 4). The lower olefin and aromatic content of C2 make it a considerably less reactive fuel than RF-A. For identical reacted amounts of carbon, the two fuels produced virtually the same amount of ozone. The was the case for most fuels. The ratio of max O_3 to ΔROG for all fuels, other than RF-L and RF-F, was 0.50 ± 0.06 ppb μg^{-1} m^3 (see Table 4). Despite having reacted the same amount of carbon and having produced the same amount of ozone, industry average gasoline produced twice as much secondary organic aerosol as did California phase II. This is because, despite the fact that ΔROG is identical for the two fuels, a much larger fraction of ΔROG for RF-A is aromatic, and as was shown before, it is that aromatic content of the fuel that is responsible for forming SOA.

Atmospheric Aerosol Formation. The data in Figure 4, excluding RF-L, can be fit rather well with the following power-law relationship:

$$\Delta M_o/\Delta\text{Aromatic} = 0.0042(\Delta M_o)^{0.6023} \qquad (4)$$

with an $r^2 = 0.997$. This suggests that if a mixture of monocyclic aromatic species is sufficiently complex, then the aerosol formed from the oxidation of that mixture can be predicted using eq 4 simply by knowing the total reacted aromatic concentration, rather than accounting for the aerosol formation potential of each aromatic species individually. Since the urban atmospheric, anthropogenic, volatile hydrocarbon (UAVHC) profile is well approximated by whole gasoline vapor, it would seem that eq 4 would be applicable for predicting SOA formation from atmospheric oxidation of UAVHC with ambient models.

Acknowledgments

We would like to acknowledge support by the U.S. Environmental Protection Agency Center on Airborne Organics, the National Science Foundation, the Coordinating Research Council, and the Chevron Corporation. T.P.W.J. would also like to acknowledge a Forschungsstipendium by the Deutsche Forschungsgemeinschaft.

Literature Cited

(1) Grosjean, D. *Atmos. Environ.* **1992**, *26A*, 953–963.
(2) Grosjean, D.; Seinfeld, J. H. *Atmos. Environ.* **1989**, *23*, 1733–1747.
(3) Turpin, B. J.; Huntzicker, J. J. *Atmos. Environ.* **1995**, *29B*, 3527–3544.
(4) Gartrell, G., Jr.; Friedlander, S. K. *Atmos. Environ.* **1975**, *9*, 279–299.
(5) Grosjean, D.; Friedlander, S. K. *J. Air Pollut. Control Assoc.* **1975**, *25*, 1038–1044.
(6) Schauer, J. J.; Rogge, W. F.; Hildemann, L. M.; Mazurek, M. A.; Simoneit, B. R.; Cass, G. R. *Atmos. Environ.* **1996**, *30*, 3837–3855.
(7) Pandis, S. N.; Paulson, S. E.; Seinfeld, J. H.; Flagan, R. C. *Atmos. Environ.* **1991**, *25A*, 997–1008.
(8) Wang, S. C.; Paulson, S. E.; Grosjean, D.; Flagan, R. C.; Seinfeld, J. H. *Atmos. Environ.* **1992**, *26A*, 403–420.
(9) Hatakeyama, S.; Izumi, K.; Fukuyama, T.; Akimoto, H.; Washida, N. *J. Geophys. Res.* **1991**, *96*, 947–958.
(10) Izumi, K.; Fukuyama, T. *Atmos. Environ.* **1990**, *24A*, 1433–1441.
(11) Stern, J. E.; Flagan, R. C.; Grosjean, D.; Seinfeld, J. H. *Environ. Sci. Technol.* **1987**, *21*, 1224–1231.
(12) Gery, M. W.; Fox, D. L.; Jeffries, H. E. *Int. J. Chem. Kinet.* **1985**, *17*, 931–955.
(13) Leone, J. A.; Flagan, R. C.; Grosjean, D.; Seinfeld, J. H. *Int. J. Chem. Kinet.* **1985**, *17*, 177–216.
(14) Grosjean. D. Aerosols. In *Ozone and Other Photochemical Oxidants;* National Academy of Sciences: Washington, DC, 1977; Chapter 3, pp 45–125.
(15) Odum, J. R.; Hoffmann, T.; Bowman, F.; Collins, D.; Flagan, R. C.; Seinfeld, J. H. *Environ. Sci. Technol.* **1996**, *30*, 2580–2585.
(16) Pankow, J. F. *Atmos. Environ.* **1994**, *28A*, 185–188.
(17) Pankow, J. F. *Atmos Environ.* **1994**, *28A*, 189–193.
(18) Hoffmann, T.; Odum, J. R.; Bowman, F.; Collins, D.; Klockow, D.; Flagan, R. C.; Seinfeld, J. H. *J. Atmos. Chem.* **1997**, *26*, 189–222.
(19) Burns, V. R.; Benson, J. D.; Hochhauser, A. M.; Koehl, W. J.; Kreucher, W. M.; Reuter, R. M. *SAE Technical Paper No. 912320*; Society of Automotive Engineers: Warren, PA, 1991.
(20) Hochhauser, A. M.; Benson, J. D.; Burns, V. R.; Gorse, R. A.; Koehl, W. J.; Painter, L. J.; Rippon, B. H.; Reuter, R. M. *SAE Technical Paper No. 912322*; Society of Automotive Engineers: Warren, PA, 1991.
(21) Paul, R. H.; Mc Nally, M. J. *SAE Technical Paper No. 902098*; Society of Automotive Engineers: Warren, PA, 1991.
(22) Kopp, V. R.; Bones, C. J.; Doerr, D. G.; Ho, S.; Schubert, A. J. *SAE Technical Paper No. 930143*; Society of Automotive Engineers: Warren, PA, 1993.
(23) Atkinson, R. *J. Phys, Chem. Ref. Data* **1994**, *Monograph 2*.
(24) Mallard, W. G.; Westley, F.; Herron, J. T.; Hampson, R. F. *NIST Chemical Kinetics Database-Version 6.01*; NIST Standard Reference Data: Gaitherburg, MD, 1994.
(25) Kwok, E. S. C.; Atkinson, R. *Atmos. Environ.* **1995**, *29*, 1685–1695.
(26) Brown, H. C.; Okamoto, Y. *J. Am. Chem. Soc.* **1958**, *80*, 4979.
(27) Forstner, H. J. L.; Flagan, R. C.; Seinfeld, J. H. *Environ. Sci. Technol.* **1997**, *31*, 1345–1358.
(28) Harley, R. A.; Hannigan, M. P.; Cass, G. R. *Atmos. Environ.* **1992**, *26*, 2395–2408.
(29) Odum, J. R.; Jungkamp, T. P. W.; Griffin, R. J., Flagan, R. C.; Seinfeld, J.H. *Science* **1997**, *276*, 96–99.

Received for review June 19, 1996. Revised manuscript received April 4, 1997. Accepted April 4, 1997.[⊗]

ES960535L

[⊗] Abstract published in *Advance ACS Abstracts,* June 1, 1997.